



HAL
open science

Nitrogen sites prevail over textural properties in N-doped carbons for the oxygen reduction reaction

Javier Quílez-Bermejo, Sara Pérez-Rodríguez, Daniel Torres, Rafael Canevesi, Emilia Morallón, Diego Cazorla-Amorós, Alain Celzard, Vanessa Fierro

► **To cite this version:**

Javier Quílez-Bermejo, Sara Pérez-Rodríguez, Daniel Torres, Rafael Canevesi, Emilia Morallón, et al.. Nitrogen sites prevail over textural properties in N-doped carbons for the oxygen reduction reaction. Journal of Colloid and Interface Science, 2024, 654, pp.446-453. 10.1016/j.jcis.2023.10.013 . hal-04274120

HAL Id: hal-04274120

<https://hal.science/hal-04274120>

Submitted on 7 Nov 2023

HAL is a multi-disciplinary open access archive for the deposit and dissemination of scientific research documents, whether they are published or not. The documents may come from teaching and research institutions in France or abroad, or from public or private research centers.

L'archive ouverte pluridisciplinaire **HAL**, est destinée au dépôt et à la diffusion de documents scientifiques de niveau recherche, publiés ou non, émanant des établissements d'enseignement et de recherche français ou étrangers, des laboratoires publics ou privés.



Distributed under a Creative Commons Attribution - NonCommercial - NoDerivatives 4.0 International License

Nitrogen sites prevail over textural properties in N-doped carbons for the oxygen reduction reaction

Javier Quílez-Bermejo^{1,2,*}, Sara Pérez-Rodríguez¹, Daniel Torres¹, Rafael Canevesi¹, Emilia Morallón³, Diego Cazorla-Amorós², Alain Celzard^{1,4}, Vanessa Fierro^{1,*}.

¹ Université de Lorraine, Centre National de la Recherche Scientifique (CNRS), Institut Jean Lamour (IJL), F-88000, Épinal, France.

² Departamento de Química Inorgánica and Instituto de Materiales, Universidad de Alicante, Ap. 99, 03080, Spain.

³ Departamento de Química Física and Instituto de Materiales, Universidad de Alicante, Ap. 99, 03080, Alicante, Spain

⁴ Institut Universitaire de France (IUF), 75231 Paris, France

- Corresponding authors : javier.quilez-bermejo@univ-lorraine.fr

vanessa.fierro@univ-lorraine.fr

Abstract

Nitrogen-doped carbon-based electrodes are among the most promising alternatives to platinum-based electrodes in the cathode of fuel cells and metal-air batteries, where the oxygen reduction reaction (ORR) takes place. Among the approaches for improving ORR activity, nitrogen functionalities and well-developed textural properties have proved very effective. Nonetheless, the question of which between nitrogen active sites or textural properties are more crucial in N-doped carbon materials remains unanswered. This work proposes a comparative and critical approach through the selective functionalization of four commercial activated carbons with different textural properties. This study highlights the greater importance of N-doping in relation to the textural properties of carbon materials, and provides fundamental insights for conclusively addressing the ongoing debate within the carbon community about the significance of these two factors in the context of ORR.

1. Introduction

The oxygen reduction reaction (ORR) in fuel cells and metal-air batteries has sluggish kinetics and high overpotential, which makes it necessary the use of high loadings of expensive electrocatalysts [1–4]. Platinum is by far the most active material towards this reaction, but its scarcity and high cost hinder the large-scale commercialization of platinum-based electrochemical devices [5–8]. One of the main alternatives is the use of metal-free carbon materials, as carbon is more abundant in nature and significantly reduces the cost of the cathode electrode [9–13]. The major limitation is the poor catalytic activity of undoped carbon materials, as they have a homogeneous charge distribution in the carbon layers, making them poorly reactive for chemisorbing and reducing oxygen molecules [14–17].

The introduction of heteroatoms or defects in general disturbs the charge density and localizes the electron density in their vicinity, which act as active sites where dioxygen molecules are attracted, chemisorbed and then reduced [18–20]. In terms of surface chemistry, introducing N functionalities into carbon materials has shown promise for enhancing ORR electrocatalysis [21–23]. It is worth mentioning here the controversy within the scientific community about active sites in N-doped carbon materials [22,23], in which graphitic and pyridinic species are proposed as the most active sites for the ORR. Besides, N-C-O-type species have been shown to be active for such a reaction [24,25]. The selective enrichment of carbon materials with graphitic-type nitrogen species has provided experimental evidence of the high efficiency of these nitrogen species in alkaline media [26].

Another interesting avenue for improving the catalytic activity of carbon materials is to tune the textural properties, as they have been shown to be crucial for the ORR performance of undoped carbon materials [27–29]. The properties of micropores, and in particular ultramicropores, go beyond transportation roles and encompass catalytic functions. Micropores serve as excellent nanoreactors in which the overlapping potential energy of the

pore walls facilitates the reduction of oxygen molecules at the interphase, leading to excellent catalytic activities. The impact of textural properties on ORR catalytic activity of undoped carbon materials has been extensively studied to conclude that the narrowest pores play a significant role in the catalytic activity of these materials [29–31].

Although these two factors have a substantial influence on the ORR electrocatalytic properties of carbon-based materials, it is worth mentioning that these parameters due to the different nature of these active sites, and cannot be easily compared. Therefore, these factors have always been examined individually, with no comprehensive study of the effect of N-doping on porous carbon materials for the ORR. Opening up new horizons in the field of carbon electrocatalysis requires a fair comparison between N functionalities and textural properties of carbon materials. Herein, the effect of textural properties on ORR catalytic activity of undoped and N-doped carbon materials is addressed through extensive physicochemical and electrochemical characterization. Four commercial activated carbons were doped using urea as the nitrogen-doping agent. The functionalization procedure led to highly selective N-doping without significantly altering the pristine textural properties, allowing a fair comparison of the role of N functionalities in N-doped carbon materials for the ORR.

2. Materials and methods

2.1 Functionalization of activated carbons

Commercial activated carbons (CAC: MSC30 and MSC20 from Kansai Coke and Chemicals Co., Ltd Japan, and CW30 and TH90I from Silcarbon) were functionalized by a two-step doping method using urea as the N-doping agent [26]. The CACs were physically mixed with urea in a 1:2 carbon-to-urea weight ratio and subjected to heat treatment at 350 °C under air flow (50 mL·min⁻¹) for 3 h, the heating rate up to this temperature being 5 °C·min⁻¹. The

materials were then thoroughly washed with water until neutral pH, and subjected to a second heat treatment under nitrogen flow ($100 \text{ mL}\cdot\text{min}^{-1}$) at $900 \text{ }^\circ\text{C}$ for 1h using a heating rate of $5 \text{ }^\circ\text{C}\cdot\text{min}^{-1}$ up to this temperature. The materials were labelled N-CAC, CAC being the name of the commercial carbon. The preparation of N-doped carbon materials is illustrated in Figure 1.

2.2 Physicochemical characterization

The structure and morphology of the samples were observed using a JEM – ARM 200F Cold FEG high-resolution transmission electron microscope (HRTEM) at 200 kV. The carbon samples were suspended in ethanol and deposited in droplets on a holey carbon grid prior to analysis. Elemental mapping was performed using energy-dispersive X-ray spectroscopy (EDX) with a JEOL spectrometer (SDD) in scanning transmission microscopy (STEM) mode. All STEM images were acquired in high-angle annular dark field (HAADF) mode. Carbon, hydrogen, oxygen and nitrogen contents were obtained using a Vario EL cube analyzer (Elementar). In this device, 2 mg of each material are burnt at about $1700 \text{ }^\circ\text{C}$ in a mixed atmosphere of helium and oxygen. The gases produced are selectively separated in a chromatographic column and quantified using a thermal conductivity detector (sensitivity $\approx 40 \text{ ppm}$), allowing the calculation of C, H and N contents initially present in the materials. In a second experiment, the oxygen content was obtained by reducing the oxygen-containing combustion gases to CO, and quantifying the latter.

The surface chemistry was also studied by X-ray photoelectron spectroscopy (XPS) in a VG-Microtech Multilab 3000 spectrometer, with a non-monochromatic Al $K\alpha$ X-ray source under vacuum. The deconvolution of the N1s spectra was performed by least-squares fitting using Gaussian-Lorentzian (20:80) curves.

Nanoscale structural order was studied for all carbon samples by Raman spectroscopy using a Horiba XploRa Raman apparatus equipped with a 50 X long-range objective. The spectra were acquired between 800 and 2000 cm^{-1} with a circularly polarized laser of wavelength 638

nm, filtered at 10% maximum energy to prevent sample heating, and using a holographic grating of 1200 lines per nm.

The textural properties of the carbon materials were studied using N₂ and H₂ adsorption, the isotherms of which were obtained at -196 °C with a 3Flex manometric sorption analyzer (Micromeritics, Atlanta, GA). Prior to adsorption measurements, the samples were outgassed under secondary vacuum at 110 °C for 24h. The BET area (A_{BET}) was calculated by applying the Brunauer-Emmet-Teller theory, using the adequate relative pressure range of the N₂ adsorption isotherm [32,33]. The NLDFT surface area (S_{NLDFT}) was calculated from the combination of both N₂ and H₂ adsorption isotherms using a 2D non-local density functional model (2D-NLDFT) available in SAIEUS software (Micromeritics, Atlanta, GA). Pore size distributions (PSDs) and cumulative pore volumes were also calculated from the combination of the two isotherms. The other textural features were obtained by integrating the PSDs, such as total pore volumes, V_T ; ultramicropore volumes (corresponding to pore diameters less than 0.7 nm), $V_{ult-micro}$; supermicropore volumes (corresponding to pore diameters between 0.7 and 2 nm), $V_{sup-micro}$; micropore volumes (pore diameters less than 2.0 nm), V_{micro} ; and mesopore volumes (pore diameters between 2.0 and 50 nm), V_{MES} .

2.3 Electrochemical characterization

ORR tests were performed using a rotating ring-disk electrode (RRDE) in a conventional three-electrode cell with an Autolab PGSTAT302 potentiostat (Metrohm, Netherlands). The working electrode was equipped with a glassy carbon disk of 5 mm diameter and a second platinum ring electrode. A reversible hydrogen electrode (RHE) immersed in the same working electrolyte and a graphite rod were used as reference and counter electrodes, respectively.

Prior to the electrochemical experiments, the glassy carbon working electrode was modified as follows [34]: 0.5 mg of the carbon material was dispersed in 0.125 mL of an aqueous solution containing 0.2 wt.% of Nafion ® and 20 wt.% of isopropanol. 4 drops of 8.42 µL were drop-cast onto the glassy carbon disk to reach a carbon loading of 0.68 mg·cm⁻².

The electrocatalytic activity towards the ORR was evaluated by linear sweep voltammetry (LSV) in an oxygen-saturated 0.1 M KOH solution at a scan rate of 5 mV s⁻¹ in the potential range of 1.0 - 0.0 V vs RHE. To calculate the number of electrons transferred (n), the platinum ring electrode was fixed at a constant potential of 1.5 V vs RHE. The equation is as follows:

$$n = \frac{4I_D}{I_D + I_R/N}$$

where the current obtained at the ring and disk (absolute value) is denoted I_R and I_D , respectively, and N is the collection efficiency of the RRDE, which was obtained experimentally by the reversible redox couple $[\text{Fe}(\text{CN})_6]^{3-/4-}$ and was determined to be 0.265.

3. Results and discussion

Figure 1 shows HRTEM images of all N-CAC samples, in which a typical disordered structure is observed in all materials, characteristic of activated carbons. In the N-CW30 sample, the presence of mesopores with a size of about 10 nm can be observed, while there are apparently only micropores in the other N-CACs. Moreover, EDX mapping analysis was also performed and Figure 1e-1h shows a homogenous distribution of nitrogen and oxygen moieties throughout the N-MS30 carbon material, confirming the successful introduction of dispersed heteroatoms by the two-step doping method.

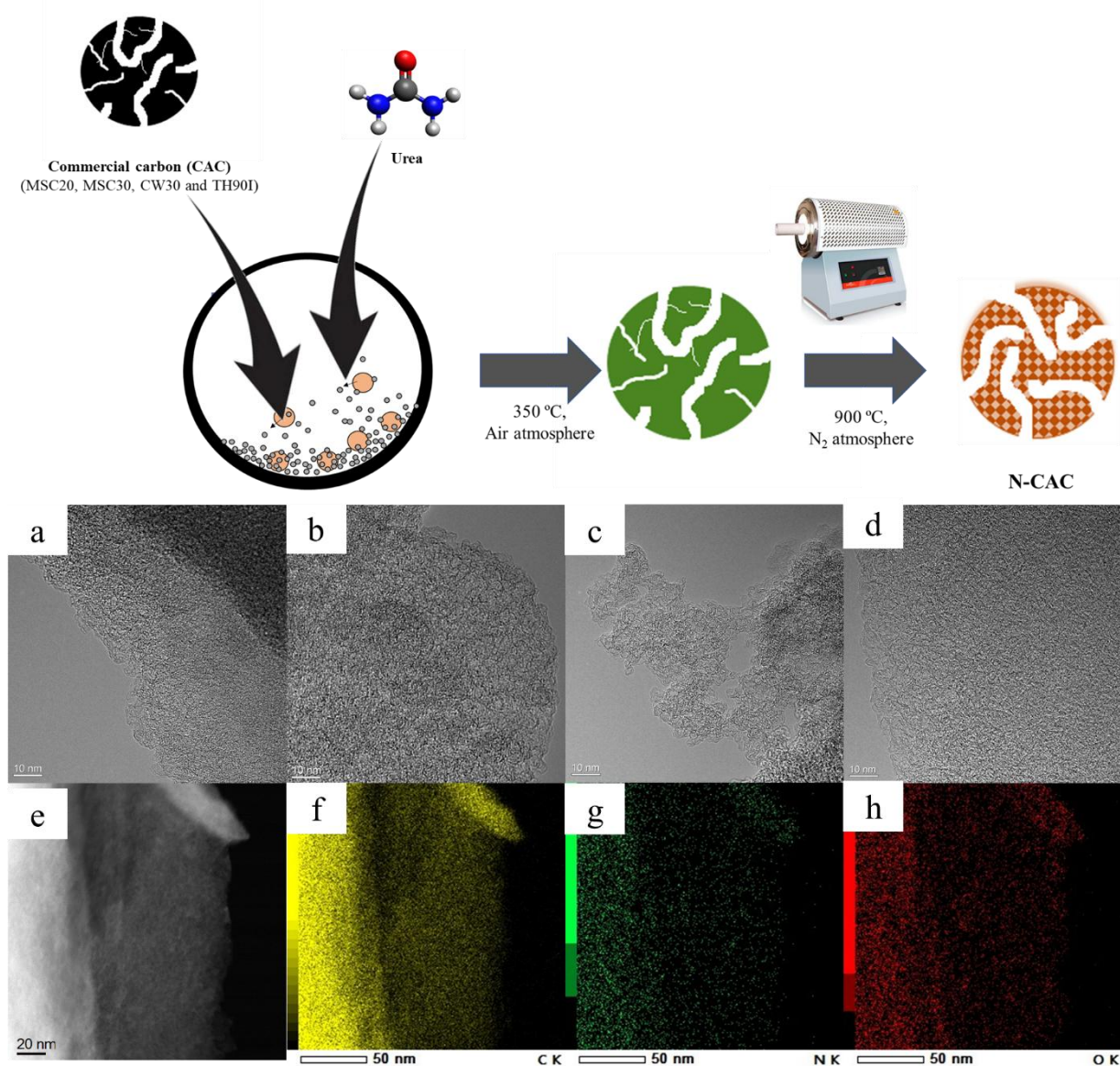


Figure 1 : (Top) Schematic illustration of urea functionalization and carbonization procedure. (Bottom) HRTEM images of (a) N-MSC20, (b) N-MSC30, (c) N-CW30, (d) N-TH90I pristine activated carbons. (e) HAADF image of N-MSC30 material and EDX mapping of the elements: (f) carbon, (g) nitrogen and (h) oxygen of the same image.

Heat treatment yields, and carbon, oxygen, hydrogen and nitrogen contents determined by elemental analysis, are gathered in Table S1 for all materials. After functionalization with urea, the heat treatment yields of N-CAC samples were highly dependent on the pristine CAC, likely due to variations in oxygen functionalities and structural order of the materials. As previously demonstrated, oxygen functionalities play a crucial role in urea functionalization by acting as reactive sites [35]. The oxygen content in CW30 decreased from 19.5 wt.% to 5 wt.% after the heat treatment at 900 °C. Moreover, it is worth mentioning that the higher the

oxygen content of the pristine CAC, the higher the N content after the 2-step doping method. This makes sense, since oxygen moieties are known to be excellent reactive points for urea [36].

Raman spectroscopy was performed to evaluate changes in structural order after N-doping. All carbon materials show the typical profile of disordered ACs with contributions related to the D₁ and G bands. The G band appears at around 1595 cm⁻¹ and is related to the vibration of crystalline graphitic carbon, whereas the D₁ band appears at around 1350 cm⁻¹ and is related to the presence of defects [37,38]. The I_D/I_G ratio serves as an indicator of structural order in amorphous carbon materials [39]. Our data indicate that an increase in N-doping is associated with a reduction in the I_D/I_G ratio, see Figure S1 which shows the correlation between I_D/I_G ratio of the pristine CAC and the final N-doping. This observation can be attributed to the enhanced efficacy of N-doping with carbon defects. If carbon materials are compared before (Figure 2a) and after the functionalization procedure (Figure 2b), slight variations can be observed in the I_D/I_G ratio, which is always higher in the materials after the functionalization strategy. This is strongly related to the post treatment at 900 °C after urea functionalization, since high temperatures in carbonization processes often increase the structural order of amorphous carbon materials through condensation and dehydration reactions. This increase is particularly noticeable for N-TH90I and N-CW30, as the pristine CACs possessed a highly disordered structure. Interestingly, after N-doping and heat treatment at 900 °C, all N-CAC samples showed similar I_D/I_G ratio of around 1.15, highlighting the similar structural order of the resulting N-CACs. Nevertheless, the slight broadening of the D band is associated with a more disordered distribution of the amorphous carbon clusters [40], suggesting the presence of a large number of defects in N-CW30 and N-MS30. Carbon rings with a number of carbon atoms other than six also tend to broaden the D band of the Raman spectra [40], which can be related to the presence of nitrogen functionalities. It is worth noting here that the

intermediate material, i.e. that obtained prior to the heat treatment at 900 °C and after urea functionalization in air, already exhibits a reduction in D-band width in the Raman spectra of the CACs. As shown in Figure S2 for the case of MSC30, the narrowing of the D band after urea functionalization in air at 350 °C indicates that the air treatment may also contribute to the removal of carbon atoms from the most disordered areas in the CACs.

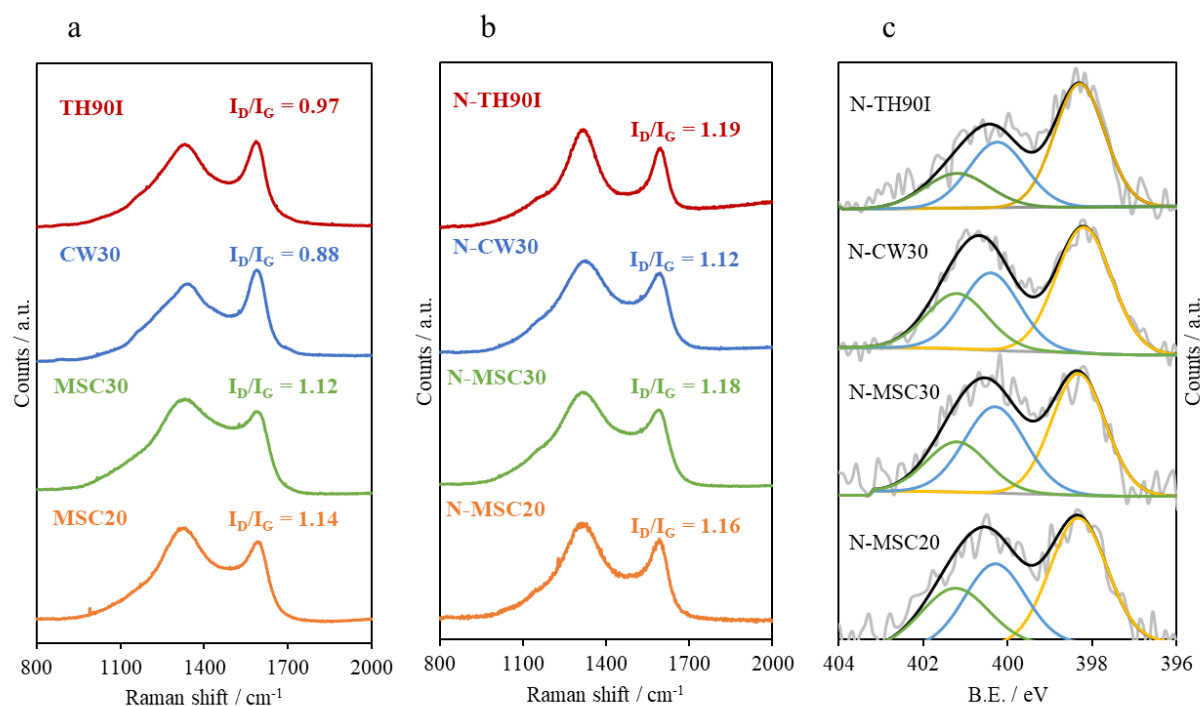


Figure 2: 1st-order Raman spectra of all (a) CAC and (b) N-CAC materials obtained at a wavelength of 638 nm. (c) N1s spectra of all carbon materials obtained after the functionalization procedure with urea and heat treatment at 900 °C. The yellow peak represents pyridinic-N species, the blue peak represents pyridonic and/or pyrrolic-N species, and the green peak represents graphitic-N species. FWHM = 1.4 - 1.8 eV.

XPS analyses were performed for all N-CACs to identify the nitrogen species and quantify the nitrogen and oxygen species on the surface of the carbon materials. Table S2 shows the atomic contents of C, O and N at the surface. As expected, the N content at the surface of the carbon materials is always higher than in the bulk (see again Table S1), since the post-functionalization of CACs with urea takes place mainly on the most accessible surface. Furthermore, there are significant differences in N contents: while N-MS20 had an N content of about 2 at.%, N-CW30 had almost double that, at around 3.8 at.%. It is worth

mentioning here that the N content at the surface followed a similar trend to that observed in the bulk. This is related to the total O content of the pristine CAC since, as mentioned above, the O moieties act as reactive sites with urea molecules, leading to a higher N content when large amounts of O groups are found in the pristine ACs [36].

Figure S3 shows full XPS spectra of N-CACs. The N1s spectra were deconvoluted in accordance with the literature [24,41]: pyridinic N species at 398.3 eV, pyrrolic and pyridonic species at 400.3 eV and graphitic (or quaternary) nitrogen at 401.2 eV. The quantification of each peak can be found in Table S2. Figure 2c shows the N1s spectra of all samples, highlighting important features of the functionalization strategy. A significant contribution from pyridinic species is observed for all materials, with also a smaller contribution of pyridonic and graphitic nitrogen. As observed, N oxidation states do not seem to have any relationship with textural properties, showing a similar N1s profile whatever the pristine CAC (Figure 2c), offering a unique opportunity to analyze the role of the textural properties of N-doped carbon materials with the same type of N species in ORR.

The textural properties of all carbon materials were characterized by N₂ (Figure 3) and H₂ adsorption isotherms (Figure S4) at -196 °C. Prior to analysis, the materials were degassed under secondary vacuum for 24 h at 110 °C. The results obtained are gathered in Table S3. Figure 3 shows the results of N₂ adsorption-desorption isotherms for CACs before and after functionalization and heat treatment. MSC30 and MSC20 are CACs with a large A_{BET} of around 2500-3000 m²·g⁻¹, while CW30 and TH90I exhibit lower values of around 1000-1500 m²·g⁻¹. It is worth noting the large mesopore volume in MSC30 and CW30, whereas MSC20 and TH90I are mainly microporous carbon materials. In detail, sample MSC20 shows a type Ia isotherm, characteristic of microporous carbon materials [33]. This is confirmed by Figure 3b, in which the pore size distribution (PSD) shows mainly the presence of micropores, around 90 % of the total pore volume. Similarly, the TH90I sample shows mainly the

presence of micropores, but has a lower surface area. On the other hand, the MSC30 sample shows a type I(b) isotherm [33], characteristic of carbon materials with a broad PSD and typical of super-activated carbons, with the presence of both micropores and narrow mesopores. This is confirmed by the PSD in Figure 3b. Sample CW30 shows a combination of type I and IV isotherms, and thus the PSD shows the existence of pores up to 3.0 nm, with a moderate A_{BET} of about $1700 \text{ m}^2 \cdot \text{g}^{-1}$. This confirms that the selected CACs exhibit significant textural differences with similar N functionalities, allowing a fair comparison of their catalytic activity taking into account only to surface area and PSD.

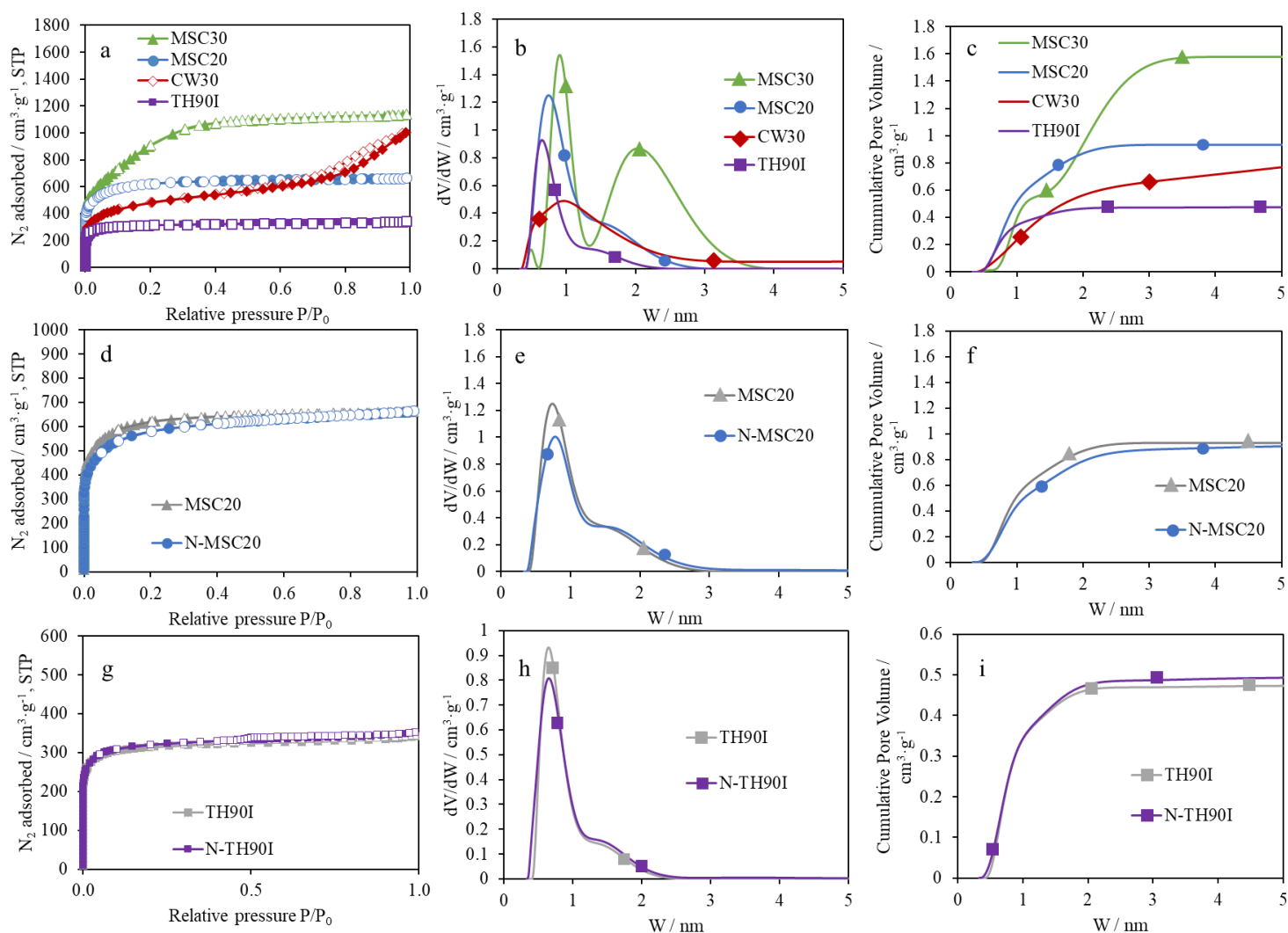


Figure 3: (a) N₂ adsorption-desorption isotherms at -196 °C (full and empty symbols stand for adsorption and desorption points, respectively), (b) pore size distributions, and (c) cumulative pore volumes of all CACs. (d) N₂ adsorption-desorption isotherms, (e) pore size distributions and (f) cumulative pore volumes of MSC20 and N-MSC20. (g) N₂ adsorption-desorption isotherms, (h) pore size distributions and (i) cumulative pore volumes of TH90I and N-TH90I.

Concerning N-CACs, N-doping did not lead to significant changes in the textural properties of the pristine CACs, especially in microporous carbon samples, i.e., MSC20 (Figure 3d-f), and TH90I (Figure 3g-i). On the other hand, MSC30 and CW30 underwent slight modifications in their textural properties, as shown in Figures S5 and S6, respectively. Here, it is worth noting that the PSD and cumulative pore volume of MSC20 (Figures 3d-f) and TH90I (Figure 3g-i) remained unchanged, while MSC30 and CW30 underwent more significant changes (Figures S5 and S6). In particular, the PSD profile of CW30 was significantly modified, leading to a defined contribution at 0.7 nm.

The N-functionalization presented here allowed similar nitrogen species to be selectively introduced into the carbon matrix, as demonstrated by XPS, while retaining most of the textural properties of the pristine CACs. Hence, these materials enable evaluation of whether surface chemical functions or textural properties are more important for ORR using N-doped carbon materials. Therefore, hereafter, the catalytic activities of N-doped and undoped CACs were evaluated as electrocatalysts for the oxygen reduction reaction.

Figure 4a shows the LSV curves for the CACs, showing moderate catalytic activity for all of them towards the ORR. However, significant differences are observed depending on their textural properties. MSC30 is the undoped CAC with the best catalytic performance in terms of E_{ONSET} (0.83 V) and limiting current density, closely followed by MSC20 and TH90I samples with an E_{ONSET} of 0.82 V. This value is typical of undoped carbon materials for ORR electrocatalysis, as observed in the literature [42,43]. Finally, CW30 sample shows poor activity ($E_{\text{ONSET}} = 0.74$ V), which is comparable to the catalytic activity of the glassy carbon disk [44].

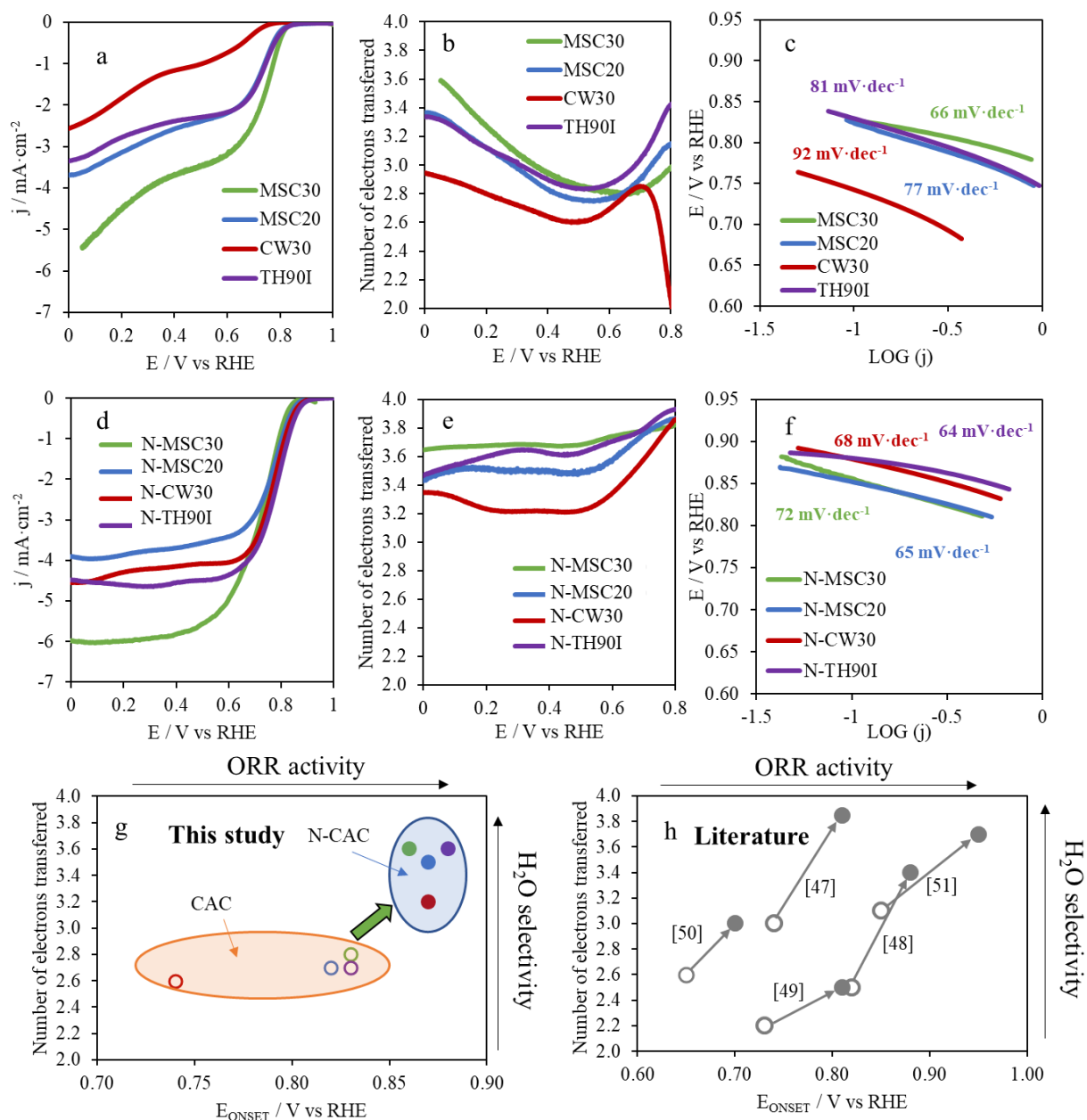


Figure 4: (a) LSV curves and (b) number of electrons transferred for pristine activated carbons. (c) Tafel slopes calculated from LSV curves for all CAC materials. (d) LSV curves, (e) number of electrons transferred and (f) Tafel slopes for N-CAC materials. Scan rate = $5 \text{ mV}\cdot\text{s}^{-1}$. Rotation speed = 1600 rpm. Electrolyte = O_2 -saturated 0.1 M KOH solution. (g) Schematic illustration of E_{ONSET} and number of electrons transferred in CAC and N-CAC materials. (h) Schematic representation of E_{ONSET} and number of electrons transferred of different N-doped carbon materials before (light grey dots) and after (dark grey dots) post-functionalization treatments in the literature.

Concerning undoped CACs, textural properties seem to be of paramount importance, with materials featuring large volumes of micropores being those exhibiting better catalytic activity for the ORR, while materials featuring large volumes of mesopores show lower catalytic activity. Furthermore, the total surface area does not seem to play a crucial role in the catalysis towards the ORR in undoped CACs. This confirms previous studies in which solely

micropores were clearly identified as responsible for the ORR in pure carbons [29,45]. Furthermore, the number of electrons transferred (Figure 4b) shows that undoped CACs exhibit a high hydrogen peroxide production (i.e., high selectivity towards the 2-electron pathway), which is not recommendable for fuel cells and metal-air batteries, as hydrogen peroxide is a strong oxidizing agent that can damage most components of these electrochemical devices. Tafel slopes were calculated from LSV curves, with only slight difference between CAC samples (see Figure 4c).

For N-CACs, N-doping led to a significant improvement of the ORR catalytic activity independently of the CAC, confirming that this N-doping method using urea and heat treatment is a promising route to induce a significant enhancement of catalytic activity. The improvement in catalytic activity is observed for all N-CACs (see Figures 4c and S7-10), and it is especially remarkable when CW30 material is used as precursor. This is not only related to the nitrogen functional groups that have been introduced into the carbon material, but also to the changes in textural properties after the doping procedure. CW30 underwent a significant structural change after N-doping and heat treatment, so it cannot be used to evaluate the relative importance of textural properties and surface chemistry since both parameters were altered during the functionalization and carbonization procedure. N-MS30 also showed significant textural differences when compared to MS30, making this material of little use for a fair comparison. In contrast, MS20 and TH90I showed almost identical textural properties to N-MS20 and N-TH90I, respectively, with the main difference being their surface chemistry, allowing an appropriate assessment of the role of N-doping in the catalytic activity for the ORR.

Figure S10 shows that the introduction of N functional groups is of paramount importance in achieving highly efficient catalytic activity with an E_{ONSET} of almost 0.90 V in N-TH90I, which is much higher compared to pristine TH90I ($E_{\text{ONSET}} = 0.82$ V). The relevance of N

functional groups in TH90I samples is also observed in the limiting current density (from $-4.5 \text{ mA}\cdot\text{cm}^{-2}$ to $-2.3 \text{ mA}\cdot\text{cm}^{-2}$ at 0.5 V vs. RHE for N-TH90I and pristine TH90I, respectively). The number of electrons transferred also clearly depends on the presence of N functional groups, showing a much higher value of n in samples doped with nitrogen species (Figure S11). In the case of TH90I, the value of n for the pristine activated carbon was around 2.7 at 0.5 V vs RHE, rising to 3.6 at the same potential after N-doping. This significant change in the value of n indicates different active sites for ORR present in TH90I and N-TH90I.

A similar trend was observed when using MSC20 (Figure 4d-f and Figure S9), with the introduction of nitrogen species improving the catalytic activity in terms of E_{ONSET} and limiting current density. The number of electrons transferred is also clearly higher when the doped materials are used, from 2.7 for pristine MSC20 to 3.5 for N-MS20. Therefore, the comparison of the ORR electrocatalytic activity of N-doped and undoped carbon materials with almost identical textural properties shows that the role of N functional groups is very important, always leading to a higher E_{ONSET} , limiting current density and, more significantly, a larger number of electrons transferred. The superior catalytic performance of N-doped carbons compared to undoped carbons has been widely associated with the presence of pyridinic and graphitic N species [46,47], although pyridonic N can also provide high catalytic performance for the ORR [25,48,49]. In N-CACs, there is a large contribution from all these nitrogen species, leading to a low overpotential for such a reaction.

As all N-CACs show the same N1s profile after the functionalization procedure and, therefore, similar surface chemistry, the role of textural properties in N-doped carbon materials can be studied by evaluating and comparing N-MS20, N-MS30, N-CW30 and N-TH90I samples. Figure 4d shows the LSV curves of all N-CACs, the main difference being their texture. Figure S12 shows that the E_{ONSET} values of all N-CACs are rather similar, suggesting that textural properties are not decisive in the kinetic region, but that the N active sites govern

their catalytic properties. To confirm further the crucial role of nitrogen active sites in the ORR, Tafel slopes were calculated from LSV curves. As observed in Figure 4f, Tafel slopes around $70 \text{ mV}\cdot\text{dec}^{-1}$ were found for all N-CACs, indicating the same rate-determining step and ORR mechanism. This reveals that ORR in N-CAC materials proceeds through the same N active sites, regardless of their textural properties. Nevertheless, the role of defects cannot be discarded in enhancing ORR activity. A similar trend is observed in the number of electrons transferred. This value is close to 4 for N-CACs, while 2-electron pathways are obtained with CACs. It should be noted that these conclusions have been drawn for porous carbon materials and cannot be extrapolated to non-porous carbon materials. Indeed, it is widely known that a certain amount of development of textural properties is required to facilitate oxygen transport from the electrolyte to the active sites. Finally, it is worth mentioning that the textural properties seem to play a role in the diffusion region through the combination of the reduction of oxygen to H_2O_2 and the subsequent reduction of hydrogen peroxide to hydroxide anion at lower potentials [29].

These results indicate that textural properties are of paramount importance for ORR when using undoped carbon materials, as shown in Figure 4a, as micropores can act as nanoreactors. In the narrowest pores, the physical adsorption forces and charge transfer between a carbon surface and adsorbed oxygen indeed result in weakening of the O-O bond, leading to dissociation of the dioxygen molecule [27]. However, if N-doped carbons are used, the nitrogen groups are more catalytically active than the micropores, resulting in a loss of dependence between catalytic activity and textural properties. The high catalytic activity and selectivity to water of nitrogen species predominates in ORR electrocatalysis, and the relevance of textural properties is reduced. The aforementioned trend can be seen in Figure 4g for the CAC and N-CAC materials, where the introduction of nitrogen results in improved catalytic activity and selectivity. This observation is further supported by the existing

literature on the post-functionalization of carbon materials [50–54], where analogous trends have been reported for all materials (see Figure 4h and Table S4).

4. Conclusions

This work provides unique insights into the effect of textural properties and nitrogen active sites in carbon materials for the oxygen reduction reaction (ORR). Selective N functionalization of four different commercial activated carbons (CACs) was performed using urea, which allowed the same type of N functional groups to be introduced into each of them. The ORR performance of CACs was dependent on their microporosity, whereas in the case of N-CACs, the dependence on textural properties was overshadowed by the higher catalytic activity of the nitrogen active sites. Based on the results presented here, we could show that the nitrogen active sites definitely prevail over the microporosity in terms of ORR catalytic activity. Furthermore, our results reveal that developing the textural properties of N-doped carbon materials does not lead to enhanced ORR activity. Instead, the N functionalities govern the ORR, relegating texture to a secondary role. These findings could potentially contribute to shedding light on the longstanding debate within the carbon community regarding countless questions about the impact of texture- enhancement techniques in N-doped carbon-based ORR electrocatalysts.

Acknowledgements: The ANR-15-IDEX-04-LUE project and the TALiSMAN and TALiSMAN2 projects funded by the European Regional Development Fund (ERDF) are gratefully acknowledged. The authors would also like to thank project PID2021-123079OB-I00 funded by MCIN/AEI/10.13039/501100011033 and “ERDF A way of making Europe”.

Finally, JQB thanks the Ministerio de Universidades, the European Union, and the University of Alicante for their financial support (MARSALAS21-21).

References

- [1] J. Quílez-Bermejo, E. Morallón, D. Cazorla-Amorós, Metal-free heteroatom-doped carbon-based catalysts for ORR. A critical assessment about the role of heteroatoms, *Carbon*. 165 (2020) 434–454.
- [2] X. Tian, X.F. Lu, B.Y. Xia, X.W.D. Lou, Advanced Electrocatalysts for the Oxygen Reduction Reaction in Energy Conversion Technologies, *Joule*. 4 (2020) 45–68.
- [3] H. Chen, X. Liang, Y. Liu, X. Ai, T. Asefa, X. Zou, Active Site Engineering in Porous Electrocatalysts, *Adv. Mater.* 32 (2020) 2002435.
- [4] R. Haider, Y. Wen, Z.F. Ma, D.P. Wilkinson, L. Zhang, Z. Yuan, S. Song, J. Zhang, High temperature proton exchange membrane fuel cells: Progress in advanced materials and key technologies, *Chem. Soc. Rev.* 50 (2021) 1138–1187.
- [5] R. Bashyam, P. Zelenay, A class of non-precious metal composite catalysts for fuel cells, *Nature*. 443 (2006) 63–66.
- [6] J. Greeley, I.E.L. Stephens, A.S. Bondarenko, T.P. Johansson, H.A. Hansen, T.F. Jaramillo, K. Rossmeisl, I. Chorkendorff, J.K. Nørskov, Alloys of platinum and early transition metals as oxygen reduction electrocatalysts, *Nat. Chem.* 1 (2009) 552–556.
- [7] A. Morozan, B. Josselme, S. Palacin, Low-platinum and platinum-free catalysts for the oxygen reduction reaction at fuelcell cathodes, *Energy Environ. Sci.* 4 (2011) 1238–1254.

- [8] J. Quílez-Bermejo, S. García-Dalí, A. Daouli, A. Zitolo, R. Canevesi, M. Emo, M.T. Izquierdo, M. Badawi, A. Celzard, V. Fierro, Advanced Design of Metal Nanoclusters and Single Atoms Embedded in C1N1-Derived Carbon Materials for ORR, HER, and OER, *Adv. Funct. Mater.* 2300405 (2023).
- [9] J. Quílez-Bermejo, S. Pérez-Rodríguez, A. Celzard, V. Fierro, Progress in the use of biosourced phenolic molecules for electrode manufacturing, *Front. Mater.* 9 (2022) 810575.
- [10] D. Liu, L. Tao, D. Yan, Y. Zou, S. Wang, Recent Advances on Non-precious Metal Porous Carbon-based Electrocatalysts for Oxygen Reduction Reaction, *ChemElectroChem.* 5 (2018) 1775–1785.
- [11] Z. Yang, H. Nie, X. Chen, X. Chen, S. Huang, Recent progress in doped carbon nanomaterials as effective cathode catalysts for fuel cell oxygen reduction reaction, *J. Power Sources.* 239 (2013) 238–249.
- [12] R. Ma, G. Lin, Y. Zhou, Q. Liu, T. Zhang, G. Shan, M. Yang, J. Wang, A review of oxygen reduction mechanisms for metal-free carbon-based electrocatalysts, *Npj Comput. Mater.* 5 (2019) 78.
- [13] A. Dessalle, J. Quílez-Bermejo, V. Fierro, F. Xu, A. Celzard, Recent progress in the development of efficient biomass-based ORR electrocatalysts, *Carbon.* 203 (2023) 237–260.
- [14] J. Quílez-Bermejo, M. Melle-Franco, E. San-Fabián, E. Morallón, D. Cazorla-Amorós, Towards understanding the active sites for the ORR in N-doped carbon materials through fine-tuning of nitrogen functionalities: an experimental and computational approach, *J. Mater. Chem. A.* 7 (2019) 24239–24250.

- [15] T. Ikeda, M. Boero, S.-F. Huang, K. Terakura, M. Oshima, J.-I. Ozaki, Carbon Alloy Catalysts: Active Sites for Oxygen reduction Reaction, *J. Phys. Chem. C.* 112 (2008) 14706–14709.
- [16] G.L. Chai, Z. Hou, D.J. Shu, T. Ikeda, K. Terakura, Active sites and mechanisms for oxygen reduction reaction on nitrogen-doped carbon alloy catalysts: Stone-wales defect and curvature effect, *J. Am. Chem. Soc.* 136 (2014) 13629–13640.
- [17] K. Gong, F. Du, Z. Xia, M. Durstock, L. Dai, Nitrogen-doped carbon nanotube arrays with high electrocatalytic activity for oxygen reduction, *Science.* 323 (2009)
- [18] M. Wu, J. Li, Z. Liu, H. Liu, G. Wang, J. Ma, Boron doped partially wrapped hierarchical porous carbon materials towards oxygen reduction reaction, *J. Electroanal. Chem.* 938 (2023) 117456.
- [19] S. García-Dalí, J. Quílez-Bermejo, J. Castro-Gutierrez, M.T. Izquierdo, A. Celzard, V. Fierro, Catalyzing sustainability: phytic acid as a green precursor for metal-free carbon electrocatalysts in ORR, *RSC Sustain.* 1 (2023) 1270–1277.
- [20] S. García-Dalí, J. Quílez-Bermejo, J. Castro-Gutierrez, N. Baccile, M.T. Izquierdo, A. Celzard, V. Fierro, Green and easy synthesis of P-doped carbon-based hydrogen evolution reaction electrocatalysts, *Carbon.* 212 (2023) 118154.
- [21] B. Wu, H. Meng, D.M. Morales, F. Zeng, J. Zhu, B. Wang, M. Risch, Z. Xu, T. Petit, Nitrogen-Rich Carbonaceous Materials for Advanced Oxygen Electrocatalysis: Synthesis, Characterization, and Activity of Nitrogen Sites, *Adv. Funct. Mater.* 32 (2022) 2204137.
- [22] K.H. Wu, D.W. Wang, D.S. Su, I.R. Gentle, A Discussion on the Activity Origin in Metal-Free Nitrogen-Doped Carbons for Oxygen Reduction Reaction and their

- Mechanisms, *ChemSusChem*. 8 (2015) 2772–2788.
- [23] S.K. Singh, K. Takeyasu, J. Nakamura, Active Sites and Mechanism of Oxygen Reduction Reaction Electrocatalysis on Nitrogen-Doped Carbon Materials, *Adv. Mater.* 31 (2019) 1804297.
- [24] J. Quílez-Bermejo, C. González-Gaitán, E. Morallón, D. Cazorla-Amorós, Effect of carbonization conditions of polyaniline on its catalytic activity towards ORR. Some insights about the nature of the active sites, *Carbon*. 119 (2017) 62–71.
- [25] R. Silva, D. Voiry, M. Chhowalla, T. Asefa, Efficient Metal-Free Electrocatalysts for Oxygen Reduction: Polyaniline-Derived N- and O-Doped Mesoporous Carbons, *J. Am. Chem. Soc.* 135 (2013) 7823–7826.
- [26] J. Quílez-Bermejo, S. Pérez-Rodríguez, R.L.S. Canevesi, D. Torres, E. Morallón, D. Cazorla-Amorós, A. Celzard, V. Fierro, Easy enrichment of graphitic nitrogen to prepare highly catalytic carbons for oxygen reduction reaction, *Carbon*. 196 (2022) 708–717.
- [27] M. Seredych, A. Szczurek, V. Fierro, A. Celzard, T.J. Bandoz, Electrochemical Reduction of Oxygen on Hydrophobic Ultramicroporous PolyHIPE Carbon, *ACS Catal.* 6 (2016) 5618–5628.
- [28] J. Encalada, K. Savaram, N.A. Travlou, W. Li, Q. Li, C. Delgado-Sánchez, V. Fierro, A. Celzard, H. He, T.J. Bandoz, Combined Effect of Porosity and Surface Chemistry on the Electrochemical Reduction of Oxygen on Cellular Vitreous Carbon Foam Catalyst, *ACS Catal.* 7 (2017) 7466–7478.
- [29] A. Gabe, R. Ruiz-Rosas, C. González-Gaitán, E. Morallón, D. Cazorla-Amorós, Modeling of oxygen reduction reaction in porous carbon materials in alkaline medium.

- Effect of microporosity, *J. Power Sources*. 412 (2019) 451–464.
- [30] Y. Liu, K. Li, B. Ge, L. Pu, Z. Liu, Influence of Micropore and Mesoporous in Activated Carbon Air-cathode Catalysts on Oxygen Reduction Reaction in Microbial Fuel Cells, *Electrochim. Acta*. 214 (2016) 110–118.
- [31] A.J. Appleby, J. Marie, Kinetics of oxygen reduction on carbon materials in alkaline solution, *Electrochim. Acta*. 24 (1979) 195–202.
- [32] J. Rouquerol, P. Llewellyn, F. Rouquerol, Is the BET equation applicable to microporous adsorbents?, *Stud. Surf. Sci. Catal.* 160 (2007) 49–56.
- [33] M. Thommes, K. Kaneko, A. V Neimark, J.P. Olivier, F. Rodriguez-Reinoso, J. Rouquerol, K.S.W. Sing, Physisorption of gases , with special reference to the evaluation of surface area and pore size distribution (IUPAC Technical Report), *Pure Appl. Chem.* 87 (2015) 1051–1069.
- [34] L. Bouleau, S. Pérez-Rodríguez, J. Quílez-Bermejo, M.T. Izquierdo, F. Xu, V. Fierro, A. Celzard, Best practices for ORR performance evaluation of metal-free porous carbon electrocatalysts, *Carbon*. 189 (2022) 349–361.
- [35] L. Sun, L. Wang, C. Tian, T. Tan, Y. Xie, K. Shi, M. Li, H. Fu, Nitrogen-doped graphene with high nitrogen level via a one-step hydrothermal reaction of graphene oxide with urea for superior capacitive energy storage, *RSC Adv.* 2 (2012) 4498–4506.
- [36] R. Pietrzak, H. Wachowska, P. Nowicki, Preparation of Nitrogen-Enriched Activated Carbons from Brown Coal, *Energy & Fuels*. 20 (2006) 1275–1280.
- [37] A. Sadezky, H. Muckenhuber, H. Grothe, R. Niessner, U. Pöschl, Raman microspectroscopy of soot and related carbonaceous materials: Spectral analysis and structural information, *Carbon*. 43 (2005) 1731–1742.

- [38] A.C. Ferrari, D.M. Basko, Raman spectroscopy as a versatile tool for studying the properties of graphene, *Nat. Technol.* 8 (2013) 235–246.
- [39] M.A. Pimenta, D. G, M.S. Dresselhaus, L.G. Cacado, A. Jorio, R. Saito, Studying disorder in graphite-based systems by Raman spectroscopy, *Phys. Chem. Chem. Phys.* 9 (2007) 1276–1291.
- [40] A.C. Ferrari, J. Robertson, Interpretation of Raman spectra of disordered and amorphous carbon, *Phys. Rev. B.* 61 (2000) 14095.
- [41] J. Quílez-Bermejo, K. Strutynski, M. Melle-Franco, E. Morallón, D. Cazorla-Amorós, On the origin of the effect of pH in ORR for non-doped and edge-type quaternary N-doped metal-free carbon-based catalysts. *ACS Appl. Mater. Interfaces.* 12 (2020) 54815-54823.
- [42] S.A. Wohlgemuth, R.J. White, M.G. Willinger, M.M. Titirici, M. Antonietti, A one-pot hydrothermal synthesis of sulfur and nitrogen doped carbon aerogels with enhanced electrocatalytic activity in the oxygen reduction reaction, *Green Chem.* 14 (2012) 1515–1523.
- [43] A. Zahoor, M. Christy, Y.J. Hwang, Y.R. Lim, P. Kim, K.S.. Nahm, Improved electrocatalytic activity of carbon materials by nitrogen doping, *Appl. Catal. B Environ.* 147 (2014) 633–641.
- [44] J. Quílez-Bermejo, A. Ghisolfi, D. Grau-Marín, E. San-Fabián, E. Morallón, D. Cazorla-Amorós, Post-synthetic efficient functionalization of polyaniline with phosphorus-containing groups. Effect of phosphorus on electrochemical properties, *Eur. Polym. J.* 119 (2019) 272–280.
- [45] M. Seredych, A. Szczurek, V. Fierro, A. Celzard, T.J. Bandosz, Electrochemical

- Reduction of Oxygen on Hydrophobic Ultramicroporous PolyHIPE Carbon, *ACS Catal.* 6 (2016) 5618–5628.
- [46] O.L. Li, S. Chiba, Y. Wada, G. Panomsuwan, T. Ishizaki, Synthesis of graphitic-N and amino-N in nitrogen-doped carbon via a solution plasma process and exploration of their synergic effect for advanced oxygen reduction reaction, *J. Mater. Chem. A* 5 (2017) 2073–2082.
- [47] J.A. Behan, E. Mates-Torres, S.N. Stamatina, C. Dominguez, A. Iannaci, K. Fleischer, M.K. Hoque, T.S. Perova, M. García-Melchor, P.E. Colavita, Untangling Cooperative Effects of Pyridinic and Graphitic Nitrogen Sites at Metal-Free N-Doped Carbon Electrocatalysts for the Oxygen Reduction Reaction, *Small* 15 (2019) 1902081.
- [48] L. Li, A. Manthiram, O- and N-Doped Carbon Nanowebbs as Metal-Free Catalysts for Hybrid Li-Air Batteries, *Adv. Energy Mater.* 4 (2014) 1301795.
- [49] J. Quílez-Bermejo, E. Morallón, D. Cazorla-Amorós, Polyaniline-derived N-doped Ordered Mesoporous Carbon Thin Films: Efficient Catalysts towards Oxygen Reduction Reaction, *Polymers* 12 (2020) 2382.
- [50] G. Zhao, L. Shi, J. Xu, X. Yan, T.S. Zhao, Role of phosphorus in nitrogen, phosphorus dual-doped ordered mesoporous carbon electrocatalyst for oxygen reduction reaction in alkaline media. *Int. J. Hydrog. Energy* 43 (2018) 1470-1478.
- [51] M.J. Mostazo-Lopez, D. Salinas-Torres, R. Ruiz-Rosas, E. Morallon, D. Cazorla-Amorós, Nitrogen-Doped Superporous Activated Carbons as Electrocatalysts for the Oxygen Reduction Reaction, *Materials* 12 (2019) 1346.
- [52] T. Zhou, R. Ma, Y. Zhou, R. Zing, Q. Liu, Y. Zhu, J. Wang, Efficient N-doping of hollow core-mesoporous shelled carbon spheres via hydrothermal treatment in

- ammonia solution for the electrocatalytic oxygen reduction reaction, *Microporous Mesoporous Mater.* 261 (2018) 88–97.
- [53] G. Tao, L. Zhang, L. Chen, X. Cui, Z. Hua, M. Wang, J. Wang, Y. Chen, J. Shi, N-doped hierarchically macro/mesoporous carbon with excellent electrocatalytic activity and durability for oxygen reduction reaction, *Carbon* 86 (2015) 108–117.
- [54] S. Lee, M. Choun, Y. Ye, J. Lee, Y. Mun, E. Kang, J. Hwang, Y. Lee, C. Shin, S. Moon, S. Kim, E. Lee, J. Lee, Designing a Highly Active Metal-Free Oxygen Reduction Catalyst in Membrane Electrode Assemblies for Alkaline Fuel Cells: Effects of Pore Size and Doping-Site Position, *Angew. Chemie - Int. Ed.* 54 (2015) 9230–9234.